Publications

Available Online

J. Sci. Res. **13** (2), 347-359 (2021)

JOURNAL OF SCIENTIFIC RESEARCH

www.banglajol.info/index.php/JSR

Gossamer-like V_2O_5 Thin Films for the Detection of Toxic Volatile Organic Compounds

G. Ravinder[1], C. J. Sreelatha[1], P. Chandar rao[1], P. Nagaraju[2], Y. Vijayakumar[2*], T. Sreekanth[3]

[1]Materials Research Laboratory, Department of Physics, Kakatiya University, Warangal, Telangana State, India

[2]Nanosensor Research Laboratory, Department of Physics, CMR Technical Campus, Kandlakoya, Medchal road, Hyderabad, Telangana State, India

[3]Deptartment of Physics, JNTUH College of Engineering Jagtial Nachupally (Kondagattu), Jagtial Dist. - 505 501, Telangana State, India

Received 21 September 2020, accepted in final revised form 12 February 2021

Abstract

Nanostructured vanadium pentoxide (V_2O_5) thin films are successfully deposited on an ultrasonically cleaned glass substrate with different deposition parameters via spray pyrolysis technique. The X-ray diffraction analysis showed that the V_2O_5 films are polycrystalline with an orthorhombic structure. SEM analysis illustrated that the gossamer-like morphology at the substrate temperature of 325 °C. The average crystallite size of the films changes from 14.29 to 23.81 nm, due to the deposition temperature enhancement. The film which is deposited at a substrate temperature of 325 °C has shown high transmittance. XPS studies validated the existence of V^{5+} oxidation form of vanadium in vanadium oxide thin film. Gas sensors are electronic devices designed to trace the concentration of different toxic gases existing in the environment. Gas sensing characterization has been performed using static liquid distribution technique towards different volatile organic compounds such as acetone, methanol, toluene and xylene. The thin film prepared at a substrate temperature of 325 °C has shown the maximum response towards 100 ppm of toluene at room temperature. The response and recovery times are determined using transient response curve, and the obtained values are 21 sec and 31 sec, respectively.

Keywords: Spray pyrolysis; V_2O_5; Thin films; Gas sensor; Toluene.

doi: http://dx.doi.org/10.3329/jsr.v13i2.49333 J. Sci. Res. **13** (2), 347-359 (2021)

1. Introduction

Toxic and hazardous gas sensors play an important role in the research areas such as human health, environmental protection and emissions control. Among these, human health is mostly influenced by air pollution, which causes numerous health issues. The core toxic gases in the air include carbon mono oxide, carbon dioxide, nitrogen dioxide, and volatile organic compounds (VOCs). The predominating VOCs contributing to the

* *Corresponding author:* yelsani.vijay@gmail.com

environmental pollution are toluene, methanol, acetone, ethanol, benzene and xylene. In these VOCs, toluene is one of the most frequently used material as a solvent and additive in many chemical and process industries. However, human confession to larger concentrations of toluene can still harmful and life-threatening. As per the Health Protection Agency (HPA), the United Kingdom, the toluene's occupational range is 50 ppm for eight hours [1,2]. Hence, there is a considerable demand for an active toluene sensor which is operating at room temperature is needed to detect and regulate the diffusion of toluene into the air.

Based on the sensing mechanism, the gas sensors are classified such as chemi-resistive, surface acoustic wave and field-effect transistor-based sensors [3]. The chemi-resistive sensors have more advantages, like immense sensitivity, selectivity and simple to connect the network. Most of the chemi-resistive gas sensors are metal oxide-based sensors, such as SnO_2, ZnO, TiO_2, WO_3, MoO_3 and V_2O_5. Among these, vanadium pentoxide has a fascinating material because of its variable oxidation states between V^{2+} and V^{5+} with large optical band gap (2.30 eV), outstanding physically and chemically stable material [4,5]. Besides of these unique characteristics, natural abundance the large specific heat capacity and comparatively low-cost makes it to a various scientific and industrial applications such as solar cell, batteries, fibre optical storage systems, laser scanners, thermochromic coatings, switching devices, ultrafast switching and IR detectors and gas sensors [6-14].

V_2O_5 thin films can be deposited using various techniques, such as pulsed laser deposition (PLD) [15], thermal evaporation [16], atomic layer deposition (ALD) [17], e-beam evaporation [18], spin coating [19], magnetron sputtering [20], dip coating [21] and spray pyrolysis technique [22]. The spray pyrolysis technique has many advantages, such as large-area deposition and high stoichiometry at a low-cost. In the spray pyrolysis technique, deposition parameter like substrate temperature (deposition temperature), nozzle to substrate distance, and the solution and flow rate concentration are crucial to get high-quality thin films. The substrate temperature has an essential component in determining the microstructure and morphologies of thin-film because of the pyrolytic decomposition energy.

In the current investigations, we have prepared gossamer-like V_2O_5 films using low-cost spray pyrolysis method and systematically characterized their microstructural, optical and gas sensing properties concerning the deposition temperatures in the range of 275 - 350 °C.

2. Materials and Methods

Vanadium pentoxide (V_2O_5) thin films were prepared on a pre-cleaned glass substrate with the low cost and simple spray pyrolysis technique with ammonium vanadate (NH_4VO_3, Sigma-Aldrich, 99 %) as a precursor material. The glass substrate cleaning procedure has been described previously [22]. The solution's concentration was kept at 0.075M, and the solvent consisting of methanol and de-ionized water with a volume ratio of 1:5. Other deposition parameters like the flow rate at 1 mL/min, deposition time is 10

min, nozzle to substrate distance is 25 cm, the air is utilized as carrier gas which is maintained at a pressure of 1 mbar, and the substrate temperature is varied at 275, 300, 325 and 350 °C. These samples are labelled as V11, V12, V13 and V14 respectively.

The thin films structural characterization has been studied by the grazing incident X-ray diffraction technique (XRD) by Bruker D8 HR-XRD system equipped with a monochromatic CuK_{α} radiation source (0.154 nm) in the range of 10°–60°. The microstructure of the vanadium pentoxide thin films was studied with the SEM (JEOL-JSM 5600) equipment. Surface topography and roughness of vanadium pentoxide thin films were examined by atomic force microscopy using Nanoscope E software with the contact mode. The Raman scattering measurements of the samples were performed with micro-Raman Spectrometer (Labram HR800) in the wavenumber range of 50–1100 cm^{-1}. UV-Visible measurement was recorded using Lambda spectrophotometer, USA, in the wavelength range of 300-850 nm. The X-ray photoelectron spectroscopy characterizations were carried using Al K-α X-ray source and Phoibos 150 electron analyzer at the Angle-Resolved Photo Electron Spectroscopy (BL-3) of Indus-1 synchrotron radiation source, RRCAT, Indore, India. The film's thickness was computed using the weight difference technique, and it was varied from 300 to 250 nm with the increasing of substrate temperature. The significant reduction in the film's thickness could be associated with the re-evaporation process of the material at comparatively larger deposition temperatures. The thin film's Adhesivity test was performed using the scotch tape method, and the thin films appeared to be good adhesive to the substrates with high uniformity and pinholes free.

The gas sensing characterization of vanadium pentoxide films was investigated with a static liquid gas distribution technique with an indigenous air-sealed gas testing chamber of 5000 mL capacity with a heater, thermocouple and electrical contacts accompanying with a high-resistance Keithley electrometer (6517B, USA) [23]. The various toxic vapours such as acetone, methanol, toluene and xylene were utilized to investigate the gas sensing characterization of V_2O_5 thin films. The sensitivity of the thin film sensor was determined with the below formula [24].

$$\text{Sensitivity } (s) = \frac{R_a}{R_g} \quad (1)$$

R_a is the sensor element's resistance in the presence of dry air, and R_g is the resistance of the sensor element in the test gas presence.

3. Results and Discussion

3.1. *X-Ray diffraction*

The X-ray diffraction investigations have been carried out to determine the crystal orientation and the crystalline behavior of the V_2O_5 thin films. X-ray diffraction patterns of the vanadium pentoxide thin films prepared at different substrate temperatures are depicted in Fig. 1. For the V11, V12, V13 and V14 samples, all the XRD peaks are

matched to an orthorhombic structure with polycrystalline nature, and these peaks are indexed with the help of joint committee on powder diffraction card number 053–0538. The crystallinity enhances the deposition temperature from 275° to 325°C, further enhancing the temperature, crystal quality decreases due to the re-crystallization transformation.

The average crystallite size of the vanadium pentoxide films along the preferred orientation (110) was determined by Scherer's equation which can be written as follows [25];

$$\text{Average Crystallite size (D)} = \frac{0.94\lambda}{\beta cos\theta} \quad (1)$$

where β is the FWHM, and λ is the monochromatic wavelength of incident X-ray radiation (λ =0.154 nm for CuKα). The dislocation density of the crystal is related to the missing of lattice planes in the crystal structure, and it can be calculated from crystallite size (D) by using the below equation [26]:

$$\text{Dislocation density } (\delta) = \frac{1}{D^2} \quad (2)$$

The lattice parameters of V_2O_5 thin films were determined with the help of the following equation [27]:

$$\frac{1}{d_{hkl}^2} = \frac{h^2}{a^2} + \frac{k^2}{b^2} + \frac{l^2}{c^2} \quad (3)$$

where, a, b and c are the lattice parameters, h, k, l are miller indices of the corresponding plane and d is the interplanar separation

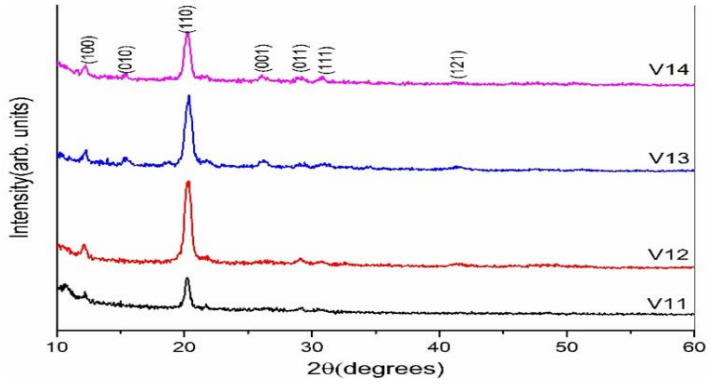

Fig. 1. XRD patterns of vanadium pentoxide thin films.

The variation of crystallite size, dislocation density and lattice parameters of the vanadium pentoxide films deposited at different deposition temperatures are tabulated in Table 1. The crystallite size of the V_2O_5 thin films is enhanced as increasing the substrate temperature to 325 °C. The increase in average crystallite size with substrate temperature is due to the optimum energy available to form larger grains. Further increasing the

temperature, crystallite size decreased due to re-crystallization takes place at higher substrate temperatures. Dislocation densities of the films are reduced with the increasing substrate temperature. The determined lattice parameters are in agreement with reported data [28].

Table 1. The lattice constants and crystallite size, dislocation density calculated from XRD data V_2O_5 thin films.

SL No.	Sample	Lattice parameter (Å)			Crystallite size (nm)	Dislocation density (10^{-3} nm^2)
		A	b	c		
1	V11	7.80	5.30	4.45	14.29	4.9
2	V12	7.27	5.55	3.07	25.36	1.6
3	V13	7.23	5.46	3.30	30.08	1.1
4	V14	7.25	5.46	3.40	22.81	1.9

3.2. *Raman spectroscopy*

The micro-Raman spectra of the V_2O_5 thin films deposited at different substrate temperatures are presented in Fig. 2. The variation in the intensity and broadening of the peaks with respect to the deposition temperature reveals the interpretation of the microstructures seemed due to higher substrate temperatures. These deviations are consigned due to lattice phonon-confinement triggered by the large crystallite sizes and changing crystallinity of the thin films. The two bands observed at 143 and 995 cm^{-1} evolve into greater intense and sharp with an enhancement of substrate temperature to 325 °C, and other observed bands are assigned in Fig. 2. The presence of these bands is evident for the formation of the high stoichiometry V_2O_5 thin films. The other Raman bands at 405 and 528 cm^{-1} are assigned to the bending modes of V= O and stretching modes of V–O–V bonds, accordingly. The Raman shift near 284 cm^{-1} is designated to the bending modes of V=O bonds. No other Raman shifts of oxygen and vanadium were remarked, which validated the monophasic composition of V_2O_5 thin film [29].

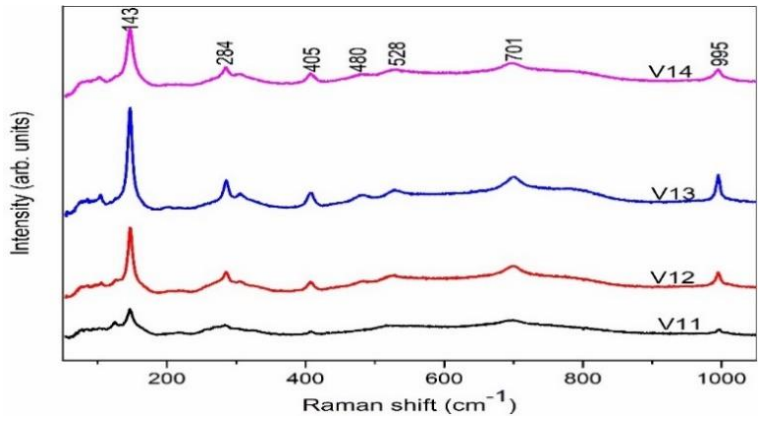

Fig. 2. Raman spectrum of V_2O_5 thin films.

3.3. *Morphological studies*

Fig. 3 shows the scanning electron microscopy (SEM) images of V_2O_5 films deposited at different substrate temperatures. The film prepared at the deposition temperature of 275 °C, is showing the small flower-like morphology due to incomplete decomposition of precursor material. As the deposition temperature is increased to 325 °C, the gossamer-like morphology is observed with a diameter of 1 μm. This type of morphology having more porosity, which is the most suitable for the application of gas sensing. The V_2O_5 thin film prepared at 350 °C of substrate temperature shows the random agglomerated morphology. This is due to the rapid decomposition at the surface of the substrate, which reduces the porous quality of the thin film.

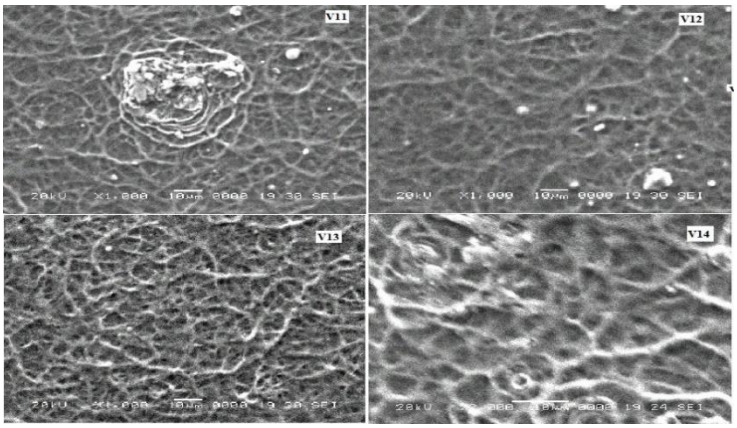

Fig. 2. scanning electron microscopy images of V_2O_5 thin films prepared at various deposition temperatures.

3.4. *Atomic force microscopy*

Fig. 4 shows the two-dimensional (2D) and three-dimensional (3D) atomic force microscopy micrographs of vanadium pentoxide thin films sprayed at different substrate temperatures. By analyzing these films using Nanoscope E software, we obtained RMS roughness of the films. The RMS roughness of the films is found to be 8, 10, 14 and 13 nm which are prepared at substrate temperatures of 275, 300, 325 and 350 °C respectively. Surface roughness increases with increasing substrate temperature up to 325 °C, then it is slightly decreased. It might be due to the size of the crystallite is reduced at that temperature. This is an essential key feature of a sensor whose large RMS roughness contributes a large surface area for chemisorption of test gas molecules on the sensor's surface.

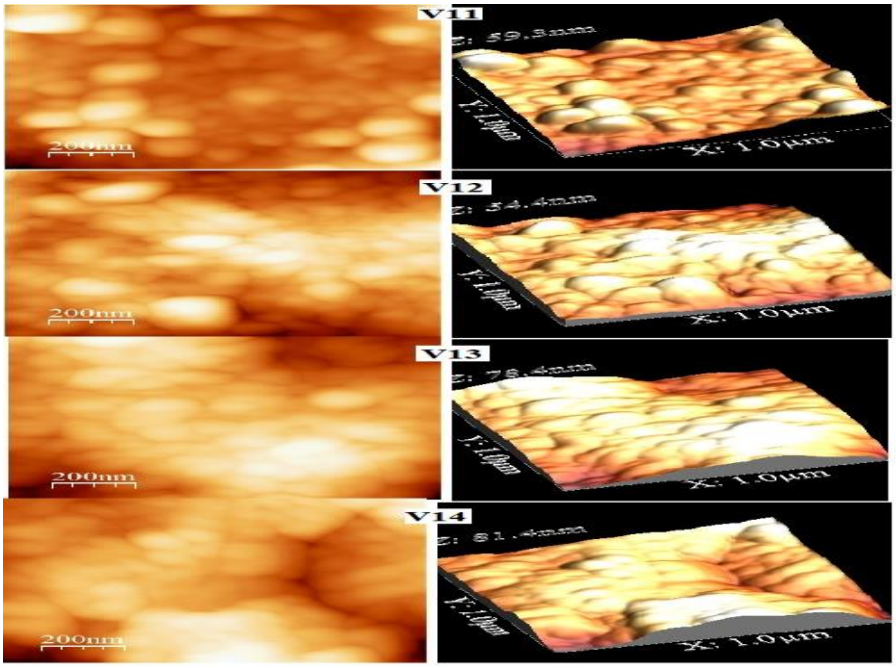

Fig. 3. AFM micrographs of vanadium pentoxide thin films.

3.5. *Optical characterization*

Fig. 5 depicts the V_2O_5 thin films optical transmittance spectra sprayed at different deposition temperatures in the wavelength range of 350 to 850 nm. The optical transmittance of the thin films increases with the increase of substrate temperature. This shows that the V_2O_5 thin films have good optical characteristics with less internal defects and high crystal quality, which is due to reduced scattering of the photon within the thin films. Tauc's direct transition plots determine the optical band gap values of the thin films from valance band to the conduction band. The optical band gap values are 2.42, 2.39, 2.35, and 2.31 eV for the V_2O_5 thin films deposited at substrate temperatures of 275, 300, 325 and 350 °C respectively. These band gap values are in good agreement with the literature data [30-32].

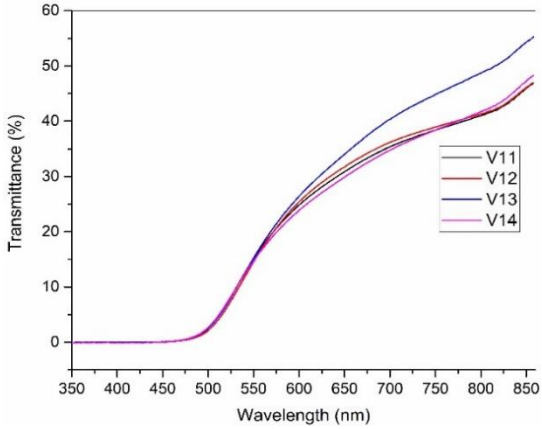

Fig. 4. Optical transmittance spectra of vanadium pentoxide thin films.

3.6. *X-ray photoelectron spectroscopic (XPS) analysis*

The XPS survey spectrum of V_2O_5 thin film deposited using spray pyrolysis technique at a deposition temperature of 325 °C(V13), as depicted in Fig. 6. The peaks corresponding to carbon (C), oxygen (O), vanadium (V), and are certainly observed in the spectrum. A peak appeared at 241 eV in the XPS spectra is due to the presence of carbon (C) which is due to the hydrocarbon contamination on the surface of the thin film while the measurements were recorded. Fig. 7 depicts the precise XPS scan of V_2O_5 film prepared at the substrate temperature of 325 °C. The deconvolution of XPS precise scan of the sample existing of three prominent peaks at different binding energies such as 516.6, 523.5 and 530 eV matching to V2p3/2, V2p1/2 and O1s respectively. These binding energy values are according to the earlier stated data [33], which also supports the existence of V^{5+} chemical form in the vanadium pentoxide thin film deposited at 325 °C**.** The peak recognized at 530 eV is designated to lattice oxygen atoms in the V_2O_5 thin film.

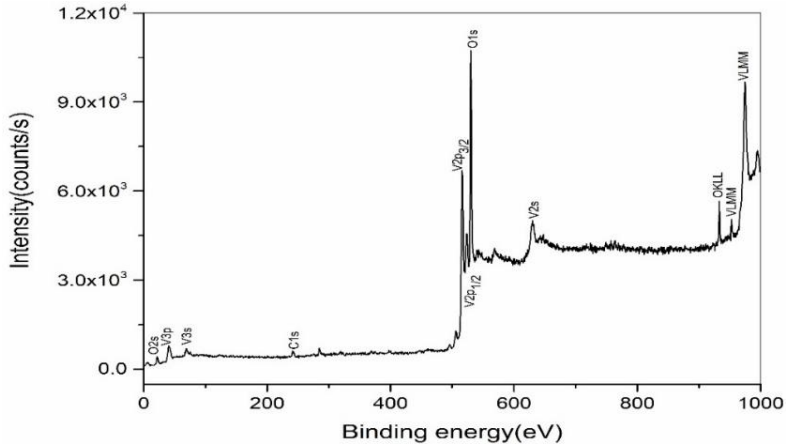

Fig. 5. XPS survey spectra of V_2O_5 thin films prepared at the deposition temperature of 325 °C.

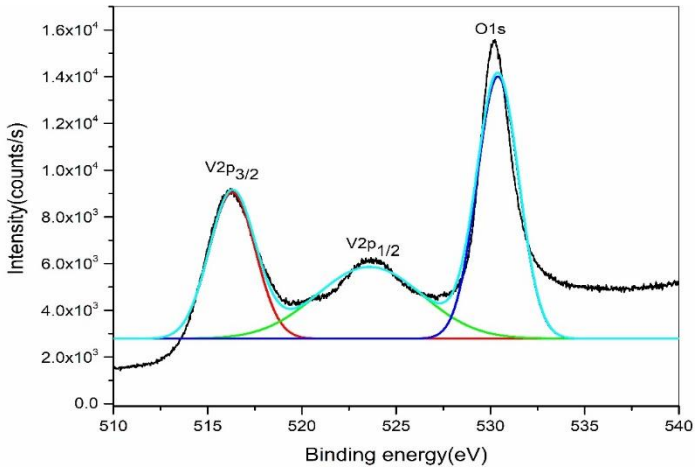

Fig. 6. XPS spectra of V2p and O1s.

3.7. *Gas sensing studies*

The metal oxide-based chemi-resistive gas sensors' sensitivity mainly depends on the change in resistance due to the influence of target gases. The stable resistance in dry air atmosphere considers as the baseline for the gas sensing properties. When the thin-film sensor is exposed to the test gases such as acetone, xylene, toluene and methanol the free electrons confined by the O_2 species will coming back to the conduction band of the thin film. Therefore, the sensor resistance is reduced, and it reached to a substantial value. Now, the sensor is exposed to the air atmosphere. The O_2 molecules are adsorbed by the vanadium oxide grains and convert as oxygen ions again; therefore, the sensor resistance is reached to baseline value [34]. The V_2O_5 sensor's selectivity is tested in the presence of different organic vapors such as acetone, methanol, toluene and xylene of 100 ppm concentration at room temperature. The responses of the different samples of V_2O_5 thin films are depicted in Fig. 8. It is observed that V_2O_5 films have shown an excellent response against toluene compared to other organic vapors. Due to the less dissociation energy of toluene might have backed for the increased sensitivity with high selectivity. Among all the V_2O_5 thin films, the film deposited at 325 °C has shown the highest response towards different volatile organic compounds due to high crystallinity and gossamer-like morphology. The transient response curve shows that the decrease and increased resistance behavior in the presence and absence of 100 ppm of toluene vapors at room temperature. The time needed by the sensor element to attain 90 % of its saturation resistance in the presence of target gas is called as response time whereas the recovery time is defined as the time taken by the sensor element to attain 10 % of saturated resistance after the removal of test gas. From the transient curve, the sensor elements' response and recovery times are 21sec and 31sec, respectively.

3.8. *Gas sensing mechanism*

The gas sensing mechanism of chemi-resistive gas sensors mainly depends on the change in electrical resistance contributed by interactions between the surface of the sensor element and test gases. In detail, when the V_2O_5 sensing element is exposed to air, adsorbed oxygen molecules captured electrons from the surface of the sensor; hence, chemi-adsorbed oxygen species were generated. These chemi-adsorbed oxygen species resulted in the formation of a depletion layer at the grain boundaries. Also, when the sensor element is exposed to a toluene gas atmosphere, the toluene molecules are adsorbed onto the thin film surface [35]. The reductive toluene vapors reacted with the chemically adsorbed oxygen ions, promoting the captured electron transition in the sensing mechanism. This process can be explained as follows.

$$C_6H_5CH_3 + O^{2-} \rightarrow C_6H_5CHO^- + H_2O + e^-$$

$$C_6H_5CHO^- \rightarrow C_6H_5CHO + e^-$$

The reduction and oxidation reactions led to decrease in the electrical potential across the depletion layer and then, a decrease in the resistance of the V_2O_5 sensor is observed. A typical toluene sensing mechanism is depicted in Fig. 10 and the comparison of different materials response times of toluene gas are tabulated in the Table 2.

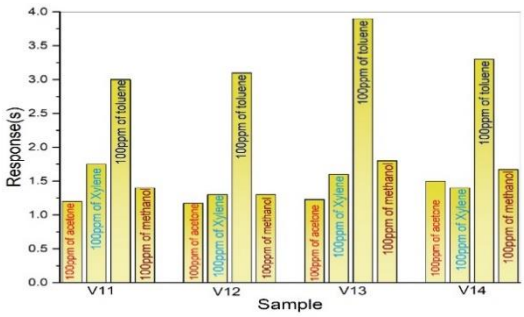

Fig. 7. The selectivity of 100 ppm of organic gases of the V_2O_5 thin films.

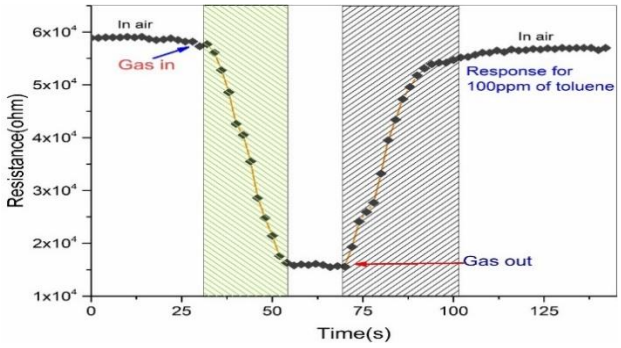

Fig. 8. Transient response of toluene with 100 ppm.

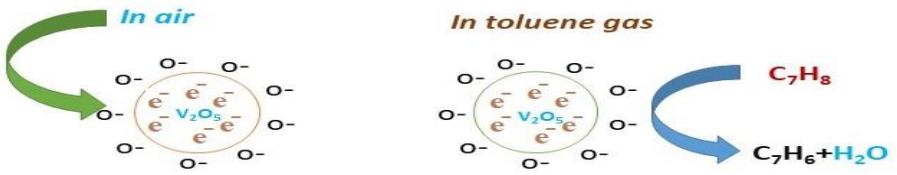

Fig. 10. Toluene sensing mechanism of V_2O_5 thin films.

Table 2. Comparison Table of response times of different materials towards toluene gas.

S.No.	Material	Operating temperature (°C)	Response time (sec)	Ref.
1	Co_3O_4	200	55	36
2	Fe_2O_3/SnO_2	90	22	37
3	Au/ZnO	377	90	38
4	V_2O_5	27	21	Present work

3. Conclusion

The V_2O_5 thin films have been deposited using spray pyrolysis technique on ultrasonically cleaned glass substrates at various substrate temperatures. X-ray diffraction, Raman spectroscopy studies confirm the formation of orthorhombic V_2O_5 phase with a layered structure. Scanning electron microscopy investigations validate the V_2O_5 thin film's gossamer-like morphology, which is deposited at a deposition temperature of 325 °C. The RMS roughness of the films is enhanced with the increase of deposition temperature. X-ray photoelectron spectroscopy survey of the film validates V^{5+} chemical form of vanadium in the V_2O_5 thin film. The V_2O_5 thin films are raised to be hugely sensitive and selective towards 100 ppm of toluene gas at room temperature. The film deposited at 325 °C is showing good response and recovery times of 21 sec and 33 sec respectively. Hence, V_2O_5 thin-film sensor is more suitable for the detection of toluene vapors at room temperature. We strongly believe that our sensor element will be used to fabricate low cost and efficient toluene sensor which can operate at field conditions in the future.

Acknowledgments

Authors G. Ravinder, RGNFD Fellowship (85825) and C. J. Sreelatha sincerely acknowledge the financial assistance No. F.530/24/DRS-II/2015 (UGC-SAP –II) to the Department of Physics, Kakatiya University. P. Nagaraju, T. Sreekanth would like to thank JNTU-Hyderabad for providing financial assistance in the form of project grant with file number JNTUH/TEQIP-III/CRS/2019/Physics/01, Y. Vijayakumar would like to thank JNTU-Hyderabad for providing financial assistance in the form of project grant with file number JNTUH/TEQIP-III/CRS/2019/Physics/03.

References

1. M. Parmar, C. Balamurugan, and D. W. Lee, Sensors **13**, 16611 (2013). https://doi.org/10.3390/s131216611
2. F. Moriarty, Environ. Pollut. **55**, 77 (1988). https://doi.org/10.1016/0269-7491(88)90163-7
3. K. Xu, C. Fu, Z. Gao, F. Wei, Y. Yiang, and C. Xu, Instru. Sci. Tech. **46**, 115 (2018). https://doi.org/10.1080/10739149.2017.1340896
4. S. Beke, Thin Solid Films, **519**, 1761 (2011). https://doi.org/10.1016/j.tsf.2010.11.001
5. C. V. Ramana, O. M. Hussain, B. S. Naidu, and P. J. Reddy, Thin Solid Films **305**, 219 (1997). https://doi.org/10.1016/S0040-6090(97)00141-7
6. A. A. Mane, P. S. Maldar, S. H. Dabhole, S. A. Nikam, and A. V. Moholkar, Measurement **131**, 223 (2019). https://doi.org/10.1016/j.measurement.2018.08.042
7. A. Mauger and C. M. Julien, AIMS Mater. Sci. **5**, 349 (2018). https://doi.org/10.3934/matersci.2018.3.349
8. Z. Luo, Z. Wu, X. Xu, M. Du, T. Wang, and Y. Jiang, Vacuum **85**, 145 (2010). https://doi.org/10.1016/j.vacuum.2010.05.001
9. S. Kumar, F. Maury, and N. Bahlawane, Mater. Today Phys. **2**, 1 (2017). https://doi.org/10.1016/j.mtphys.2017.06.005
10. J. Xia, C. Yuan, and S. Yanagida, ACS Appl. Mater. Interfaces **2**, 2136 (2010). https://doi.org/10.1021/am100380w
11. F. P. Gökdemir, O. Özdemir, and K. Kutlu, Electrochimica Acta **121**, 240 (2014). https://doi.org/10.1016/j.electacta.2013.12.164
12. Yinlu Sun, Zhiping Xie,Yanwei Li, RSC Adv. **8**, ID 39371 (2018). https://doi.org/10.1039/C8RA07326K
13. A. Subrahmanyam, Y. B. K. Redd, and C. L. Nagendra, J. Phys. Appl. Phys. **41**, ID 195108 (2008). https://doi.org/10.1088/0022-3727/41/19/195108
14. Y. Zhou, X. Chen, C. Ko, Z. Yang, C. Mouli, and S. Ramanathan, IEEE Electron Device Lett. **34**, 220 (2013). https://doi.org/10.1109/LED.2012.2229457
15. K. Panigrahi, P. Howli, and K. K. Chattopadhyay, Electrochimica Acta **337**, 135701 (2020). https://doi.org/10.1016/j.electacta.2020.135701
16. C.-C. Wang, C.-L. Lu, F.-S. Shieu, and H. C. Shih, Chem. Phys. Lett. **738**, 136864 (2020). https://doi.org/10.1016/j.cplett.2019.136864
17. C. C. Wang, K. C. Chen, F. S. Shieu, and H. C. Shih, Chem. Phys. Lett. **729**, 24 (2019). https://doi.org/10.1016/j.cplett.2019.05.018
18. O. M. Hussain and P. Rosaiah, AIP Conf. Proc. **1451**, 236 (2012).
19. G. Ravinder, C. J. Sreelatha, V. Ganesh, M. Shkir, M. Anis, and P. C. Rao, Mater. Res. Express **6**, ID 096403 (2019). https://doi.org/10.1088/2053-1591/ab2992
20. M. S. B. de Castro, C. L. Ferreira, and R. R. de Avillez, Infrared Phys. Technol. **60**, 103 (2013). https://doi.org/10.1016/j.infrared.2013.03.001
21. Y. Vijayakumar, R. Sayanna, and M. V. R. Reddy, Asian J. Appl. Sci. **7**, 753 (2014). https://doi.org/10.3923/ajaps.2014.753.760
22. Y. Vijayakumar, G. K. Mani, D. Ponnusamy, P. Shankar, A. J. Kulandaisamy, K. Tsuchiya, J. B. B. Rayappan, and M. V. R. Reddy, J. Alloys Comp. **731**, 805 (2018). https://doi.org/10.1016/j.jallcom.2017.10.056
23. V. K. Tomer and S. Duhan, Sensors Actuators B: Chem. **223**, 750 (2016). https://doi.org/10.1016/j.snb.2015.09.139
24. P. Nagaraju, Y. Vijayakumar, G. L. N. Reddy, and M. V. R. Reddy, J. Mater. Sci. Mater. Elec. **29**, 11457 (2018). https://doi.org/10.1007/s10854-018-9238-2
25. P. Nagaraju, Y. Vijayakumar, D. M. Phase, R. J. Choudary, and M. V. R. Reddy, J. Mater. Sci. Mater. Elec. **27**, 651 (2016). https://doi.org/10.1007/s10854-015-3801-x
26. S. Thanikaikarsan, T. Mahalingam, M. Raja, T. Kim, and Y. D. Kim, J. Mater. Sci. Mater. Elec. **20**, 727 (2009). https://doi.org/10.1007/s10854-008-9794-y

27. Y. Zou and H. Zhang, J. Alloys Compd. **790**, 164 (2019). https://doi.org/10.1016/j.jallcom.2019.03.176
28. Y. Zhang, Z. Zou, J. Liu, S. Zhang, and H. Zhang, Mater. Technol. **35**, 887 (2020). https://doi.org/10.1080/10667857.2019.1710338
29. C. Bhandari and W. R. L. Lambrecht, Phys. Rev. B, **89**, ID 045109 (2014). https://doi.org/10.1103/PhysRevB.89.239903
30. M. Mousavi, A. Kompany, N. Shahtahmasebi, and M. M. B. Mohagheghi, Adv. Manufact. **1**, 320 (2013). https://doi.org/10.1007/s40436-013-0045-y
31. N. H. Sheeba, A. Namitha, K. M. Ramsiya, T. M. Ashitha, and R. Suhail, J. Sci. Res. **13**, 9 (2021). https://doi.org/10.3329/jsr.v13i1.47240
32. M. A. Mahadik, S. S. Shinde, S. S. Kumbhar, H. M. Pathan, K. Y. Rajpure, and C. H. Bhosale, J. Photochem. Photobio. B: Biol. **142**, 43 (2015). https://doi.org/10.1016/j.jphotobiol.2014.09.021
33. E. Hryha, E. Rutqvist, and L. Nyborg, Surface Interface Anal. **44**, 1022 (2011). https://doi.org/10.1002/sia.3844
34. G. K. Mani and J. B. B. Rayappan, Sens. Actuators B Chem. **198**, 125 (2014). https://doi.org/10.1016/j.snb.2014.02.101
35. P. Nagaraju, Y. Vijayakumar, M. V. R. Reddy, and U. P. Deshpande, RSC Adv. **9**, 16515 (2019). https://doi.org/10.1039/C9RA02356A
36. L. Wang, J. Deng, Z. Lou, and T. Zhang, Sens. Actuators B **201**, 1 (2014). https://doi.org/10.1016/j.snb.2014.04.074
37. T. Wang, Z. Huang, Z. Yu, B. Wang, H. Wang, P. Sun, H. Suo, Y. Gao, Y. Sun, T. Li, and G. Lu, RSC Adv. **6**, 52604 (2016). https://doi.org/10.1039/C6RA05313K
38. K. Suematsu, K. Watanabe, A. Tou, Y. Sun, and K. Shimanoe, Anal. Chem. **90**, 1959 (2018). https://doi.org/10.1021/acs.analchem.7b04048